Control of Lasing in Biomimetic Structures with Short-Range Order

Heeso Noh, Jin-Kyu Yang, Seng Fatt Liew, Michael J. Rooks, Glenn S. Solomon, and Hui Cao

Phys. Rev. Lett. **106**, 183901 — Published 5 May 2011

DOI: 10.1103/PhysRevLett.106.183901

Control of lasing in biomimetic structures with short-range order

Heeso Noh[1], Jin-Kyu Yang[1], Seng Fatt Liew[1],
Michael J. Rooks[1], Glenn S. Solomon[2], Hui Cao[1,3]
[1]*Department of Applied Physics, Yale University, New Haven, CT 06520*
[2]*Joint Quantum Institute, NIST and University of Maryland, Gaithersburg, MD 20899*
[3]*Department of Physics, Yale University, New Haven, CT 06520*

Abstract

We demonstrate lasing in photonic amorphous structures that mimic the isotropic nanostructures which produce non-iridescent color in nature. Our experimental and numerical studies reveal that lasing becomes most efficient at certain frequencies, due to enhanced optical confinement by short-range order. The optimal lasing frequency can be tuned by adjusting the structure factor. This work shows that lasing in nanostructures may be effectively improved and manipulated by short-range order.

PACS numbers: 42.25.Bs; 42.70.Qs; 42.55.Zz

Over the past decade, lasing has been realized in various types of nanostructures. The most common one is the photonic crystal laser [1]. The feedback for lasing is provided by Bragg scattering of light in a periodic structure. The lasing modes are either bandedge states or defect states within a bandgap. Another type is the random laser [2, 3]. The feedback mechanism is multiple scattering of light in a disordered structure. Typically the scattering strength is nearly constant within the gain spectrum of the active medium, thus lasing is preferred at the frequency near the maximum gain. Recently, scattering resonances of monodisperse spheres were employed to tune the lasing frequency away from the peak of the gain spectrum [4]. Disorder-induced localized states inside a bandgap or near a bandedge of a photonic crystal have also been explored for lasing process [5, 6]. In between the periodic and random systems lie quasi-periodic structures that have orientational symmetry but not translational symmetry. Lasing action due to optical feedback from quasi-periodicity has been demonstrated [7–10]. More recently, deterministic aperiodic structures with pseudo-random morphologies were shown to support localized lasing modes at predictable frequencies and locations [11]. Such structures are constructed following deterministic generation rules and possess long-range order.

There is another type of photonic structure that has only short-range order but no long-range order. It is called a photonic amorphous structure (PAS). Similar to the electronic bandgap of an amorphous semiconductor, a photonic bandgap (PBG) may exist in the PAS due to coupling of the Mie resonance [12–17] or local structural uniformity [18–21]. Even when the refractive index contrast is too low to form a PBG, light scattering and transmission can be strongly modified in a PAS [22, 23]. In nature, PAS has been widely used to produce non-iridescent color (color that does not change with viewing angle) as a result of structural isotropy [24, 25]. Short-range order sets a characteristic length scale for spatial variations of the refractive index. Light scattering is enhanced at wavelengths commensurate with this dominant length scale, resulting in coloration. Biomimetic samples have been fabricated by self-assembly of colloidal particles [26, 27], and display non-iridescent color that is amenable to potential applications in photonic coatings, cosmetics and textiles [28–30].

Despite the growing interests in PAS, lasing in such structures has not been explored. Can the short-range order be used to improve light confinement and reduce the lasing threshold? Can this be done even without a PBG due to absence of strong Mie resonance or low refractive index contrast? Is it possible to control the lasing property by tailoring the

structural factor? To answer these questions, we fabricated biomimetic samples in a slab geometry with semiconductor. With optical pumping, lasing is realized in the PAS. The structural parameters are varied over a broad range in the experimental and numerical studies of lasing behavior. Despite the lack of a PBG, lasing becomes the most efficient at the wavelength corresponding to the structural correlation length as a result of enhanced scattering.

The two-dimensional (2D) PAS was generated from computer simulations of jammed packing of polydisperse cylinders [20]. The diameters of all cylinders were then reduced to the same value to eliminate the size variation. The final configuration has structural disorder only in the position of the cylinders. Next the computer-generated pattern was transfered to a GaAs membrane. A 190-nm-thick GaAs layer and a 1000-nm thick $Al_{0.75}Ga_{0.25}As$ layer were grown on a GaAs substrate by molecular beam epitaxy. Inside the GaAs layer there are three uncoupled layers of InAs quantum dots (QDs), equally spaced by 25 nm GaAs barriers. An amorphous array of air holes was fabricated in the GaAs layer by electron-beam lithography and reactive ion etching. The $Al_{0.75}Ga_{0.25}As$ layer was then selectively etched to leave a free-standing GaAs membrane in air. We fabricated patterns with different structural parameters, e.g., the radius of the circular air holes r, and the average distance a of adjacent air holes.

Figure 1(a) is a top-view scanning electron microscope (SEM) image of an array of air holes in a GaAs membrane. We performed a 2D Fourier transform of the real structure extracted from the top-view SEM image. The power Fourier spectrum displays a circular ring pattern in the inset of Fig. 1(b). It reveals (i) the structure is isotropic, (ii) there exists a dominant spatial frequency q_0 that corresponds to the radius of the ring. The characteristic length scale of the structure is $2\pi/q_0 = 255$ nm, which is equal to a. We also calculated the 2D spatial correlation function $C(\Delta\mathbf{r})$ of the fabricated pattern. It consists of isotropic rings whose amplitudes decrease with increasing spatial separation $\Delta r \equiv |\Delta\mathbf{r}|$. Figure 1(b) plots the azimuthal-averaged $C(\Delta r)$, which exhibits a damped oscillation. The peak amplitude decays exponentially with Δr. The decay length ξ, obtained from an exponential fitting, is about 480 nm. Since ξ is about $2a$, the structure has only short-range order.

The lasing experimental setup is similar to that in ref. [11]. The InAs QD emission spectrum is inhomogeneously broadened from 920 nm to over 1000 nm. Figure 2(a) shows a time-integrated emission spectrum. It consists of many sharp peaks. The intensity of an

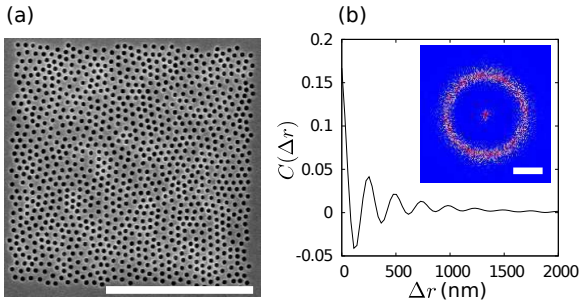

FIG. 1. (a) Top-view SEM image of a photonic amorphous structure consisting of a 2D array of air holes in a free-standing GaAs membrane. The lateral dimension of the array is 8.5 μm. There are 1024 air holes with $a = 255$ nm and $r/a = 0.3$. The white scale bar is 5 μm. (b) Inset: spatial Fourier spectrum of the structure in (a) displays an isotropic ring pattern. The scale bar is 0.003 nm^{-1}. Main panel: spatial correlation function $C(\Delta r)$ of the structure in (a) exhibits a damped oscillation with spatial separation Δr.

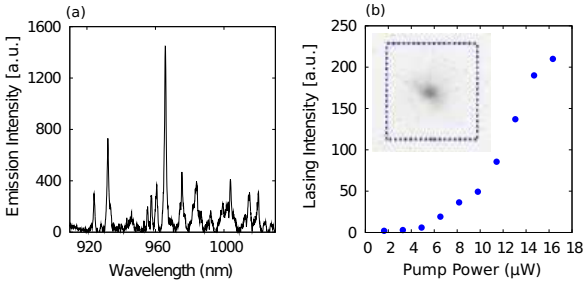

FIG. 2. (a) Measured emission spectrum from a PAS in the GaAs membrane containing InAs QDs. $a = 235$ nm, and $r/a = 0.3$. The incident pump power $P = 16$ μW. (b) Emission intensity of a peak at $\lambda = 930$ nm vs. P. The lasing threshold is $P \sim 8$ μW. Inset: an optical image of the lasing mode at $P = 16$ μW. The blue dashed square marks the border of the PAS with lateral dimension 8.5 μm.

emission peak at $\lambda = 930$ nm is plotted against the incident pump power P in Fig. 2(b). A threshold behavior is seen. When the pump power P exceeds 8 μW, the emission intensity increases much more rapidly. The linewidth of the peak also decreases dramatically with P (not shown). Such behavior indicates the onset of lasing action. The inset of Fig. 2(b) is an optical image of this mode taken at $P = 16$ μW. It shows that the lasing mode is spatially localized near the center of the pattern. The lateral dimension of the mode is about 1.4 μm.

At higher pump power, we observed multiple lasing modes across the gain spectrum of the InAs QDs.

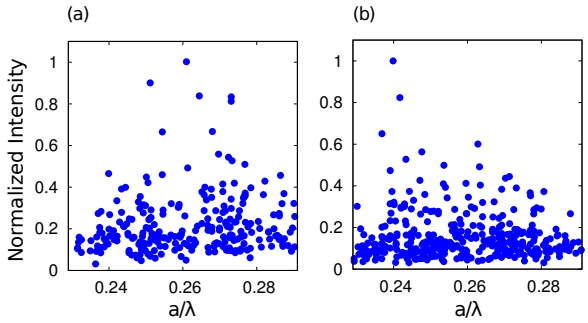

FIG. 3. Measured intensities of lasing peaks from three PAS of $a = 235$ nm, 255 nm and 275 nm. The filling fraction of air holes $f = 0.33$ in (a) and 0.28 in (b). Laser emission intensity reaches the maximum at the normalized frequency $a/\lambda = 0.26$ in (a) and 0.24 in (b).

To characterize the effect of short-range order on lasing, we can either measure the threshold of individual lasing modes at different wavelength, or compare the intensity of different lasing modes at the same pumping level. In principle, the spectral variation of the gain coefficient and mode competition for the gain would influence the lasing threshold and emission intensity. However, the gain spectrum of InAs QDs is very broad, and the gain coefficient has little variation over a wide spectral range. More importantly, the gain spectrum is dominated by inhomogeneous broadening, which significantly weakens mode competition. Hence, the interaction of lasing modes at different wavelengths or spatial location is negligible. To increase the range of the normalized frequency $\omega a/2\pi c = a/\lambda$, we probed lasing in a series of patterns of different a. The ratio of r over a was kept constant, so that the filling fraction f of air holes does not change. Figure 3(a) plots the intensities of numerous lasing modes collected from three arrays of $a = 235$ nm, 255 nm and 275 nm. The incident pump power was fixed at 16 μW. The pump spot was scanned across the interior of each array to probe lasing modes at different locations. The diameter of the pump spot was kept at 1.2 μm. As a/λ increases from 0.23 to 0.29, the lasing mode intensity first increases and then decreases. It reaches the maximum at $a/\lambda = 0.26$. Thus lasing becomes the strongest, or equivalently the lasing threshold is the lowest at $a/\lambda = 0.26$. Next we changed the filling fraction of air holes f from 0.33 to 0.28 by varying r/a, and measured three samples with $a = 235$ nm, 255 nm and 275 nm. As shown in Fig. 3(b), the maximum intensity of the lasing modes shifted

to $a/\lambda = 0.24$. These results confirm that there exists an optimal frequency for lasing in the PAS, and its value can be tuned by adjusting the structural parameters.

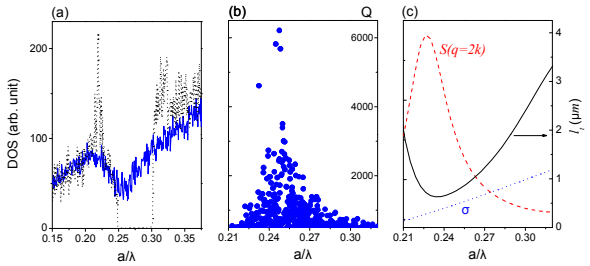

FIG. 4. (a) Calculated DOS of an amorphous array (blue solid line) and a periodic array (black dotted line) of air cylinders with $r/a = 0.28$ and $n_w = 2.83$. (b) Q factor of resonant modes in the PAS whose structural parameters are identical to those of Fig. 3(a). (c) Estimated transport mean free path l_t (black solid curve) and the structure factor $S(q = 2k)$ (red dashed curve) of the PAS. The blue dotted curve is the total scattering cross section σ of a single air cylinder embedded in a dielectric host.

To interpret the experimental data, we first calculated the density of optical states (DOS) using the order-N method [20]. The perforated GaAs membrane is approximated as a 2D structure of infinitely long air cylinders embedded in a uniform dielectric host of refractive index n_w. The value of n_w is obtained by matching the PBG of a triangle lattice of air holes in the GaAs membrane (with same density and size of air holes as in the PAS) to that of the approximate 2D structure. We consider only the transverse-electric (TE) polarization (electric field perpendicular to the air cylinder axis), because the laser emission is TE polarized. Figure 4(a) compares the DOS of a PAS to that of a periodic structure with identical r/a. The former has only a dip but not a gap, indicating that the DOS is reduced but not depleted in the PAS. This is distinct from the periodic structure which has a depleted region of DOS.

Next we calculate the resonant modes in the PAS using the finite-difference frequency-domain (FDFD) method. Figure 4(a) reveals a dramatic enhancement of the quality (Q) factor for modes at frequencies around the dip of DOS. When the air filling fraction f is reduced, the maximal Q shifts to a lower frequency. This trend agrees qualitatively to that of the strongest laser emission intensity observed experimentally [Fig. 3]. However, the maximum occurs at a slightly different frequency, due to the 2D approximation in the

numerical simulation and uncertainty in determining the refractive index of GaAs at low temperature. Note that the 2D simulation only takes into account light leakage through the edges of an array. Experimentally, light can also escape through the top or bottom surface of the GaAs membrane. The vertical leakage is included in our 3D finite-difference time-domain (FDTD) simulation of a free-standing GaAs membrane. For the PAS, the total Q factor (including both lateral and vertical leakage) displays a similar trend to that in Fig. 4(b). However, the actual Q value is notably lower than that in Fig. 4 due to vertical leakage. Hence, the variation of Q with a/λ is determined by the lateral leakage. The existence of the Q maximum indicates that light confinement is the strongest at a specific wavelength λ that scales with the characteristic length scale a of the structure. Thus the Q enhancement originates from the short-range order. Since stronger optical confinement increases the dwell time of light in the structure, light experiences more amplification and the lasing threshold is reduced. In other words, the maximum of the Q factor leads to a minimum of the lasing threshold, or equivalently, a maximum of laser emission intensity at a fixed pump power above the threshold.

Since there is no PBG in our PAS, the high-Q modes cannot be attributed to the defect states inside a gap [5, 17]. To illustrate the physical mechanism of Q enhancement, we estimate the transport mean free path l_t [31], which is a measure of the scattering strength.

$$l_t(\lambda) = \left(\frac{\pi}{k^6} \int_0^{2k} \rho F(q) S(q) q^3 dq \right)^{-1}, \tag{1}$$

where q is the spatial frequency of the structure, $F(q)$ is the form factor, $S(q)$ is the structure factor, ρ is the density of scatterers, and k is the wave vector. $k = 2\pi n_e/\lambda$, where λ is the wavelength in vacuum, and n_e is the effective index of refraction of the 2D structure. If the structure is completely random, $S(q)$ becomes 1. For the PAS, we compute the structure factor from the center position of air holes. Since the structure is isotropic, S depends only on the magnitude of $\mathbf{q}$. $F(q)$ is obtained from the differential scattering cross section of a single air cylinder (infinitely long) embedded in a dielectric host of refractive index n_w. n_e is estimated by the Maxwell-Garnett formula with the air filling fraction f.

In Fig. 4(c), l_t displays a dramatic dip that nearly coincide with the peak of Q in frequency [Fig. 4(b)]. This suggests that optimal light confinement is caused by the strongest scattering. To find the origin of enhanced light scattering, we calculate the total scattering cross section σ of a single air cylinder. It increases monotonically with a/λ, and does not

exhibit any resonant behavior within the frequency range considered [Fig. 4(c)]. Hence, the minimum of l_t is not caused by the Mie resonance of individual scatterers. In the same figure, we also plot $S(q)$ for the backscattering $q = 2k$. Its value is peaked near the dip of l_t, confirming that short-range order enhances backscattering and shortens l_t [23]. Similar results are obtained for the PAS of different f. At lower f, the minimum of l_t moves to lower frequency, consistent with the shift of Q maximum [Fig. 4(b)] and the strongest laser emission intensity [Fig. 3(b)]. Note that in the estimation of l_t with Eq.(1), the near-field coupling of adjacent scatterers is neglected. Within the frequency range of interest, there is no scattering resonance of individual air cylinders, thus the coupling of neighboring cylinders via evanescent wave is weak.

In summary, inspired by color generation by photonic amorphous structures (PAS) in nature, we fabricated biomimetic samples and investigated the lasing behavior. Although there is no photonic band gap, lasing becomes the most efficient, i.e., the laser emission becomes the strongest, at certain wavelength that can be tuned by the structure factor. This phenomenon is attributed to a dramatic enhancement of the optical confinement or Q factor. Because the PAS is isotropic, light can be confined in all directions via scattering, and the lasing modes are spatially localized. The strong frequency variation of the transport mean free path illustrates that light scattering is greatly enhanced in the PAS at specific frequencies. This enhancement is caused by the short-range order, according to our analysis of the structure factor and form factor. Consequently, the lasing threshold is lowered, and the laser emission intensity is increased at those frequencies. This study demonstrates that lasing in nanostructures can be manipulated by the short-range order.

We thank Professor Corey S. O'Hern and Carl Schreck for useful discussion and computer generation of the amorphous patterns. This work is funded by NSF Grant No. DMR-0808937 and by seed funding from the Yale NSF-MRSEC (DMR-0520495). J.-K. Yang acknowledges the support of the National Research Foundation of Korea Grant NRF-2009-352-C00039.

[1] *Roadmap on Photonic Crystals*, edited by S. Noda and T. Baba (Kluwer Academic Publishers, Dordrecht, 2003).

[2] H. Cao, in *Progress in Optics*, Vol. 45, edited by E. Wolf (Elsevier Science B. V., Amsterdam,

Netherlands, 2003) pp. 317–370.

[3] D. S. Wiersma, Nat. Phys. **4**, 359 (2008).

[4] S. Gottardo, R. Sapienza, P. D. Garcia, A. Blanco, D. S. Wiersma, and C. Lopez, Nat. Photon. **2**, 429 (2008).

[5] C. Conti and A. Fratalocchi, Nature Phys. **4**, 794 (2008).

[6] A. Yamilov and H. Cao, Phys. Rev. A **69**, 031803 (2004).

[7] M. Notomi, H. Suzuki, T. Tamamura, and K. Edagawa, Phys. Rev. Lett. **92**, 123906 (2004).

[8] K. Nozaki and T. Baba, Appl. Phys. Lett. **84**, 4875 (2004).

[9] H. J. Kim, Y.-G. Roh, and H. Jeon, Jpn. J. Appl. Phys. **44**, L1259 (2005).

[10] L. Mahler, A. Tredicucci, F. Beltram, C. Walther, J. Faist, H. E. Beere, D. A. Ritchie, and D. S. Wiersma, Nat. Photon. **4**, 165 (2010).

[11] J.-K. Yang, S. V. Boriskina, H. Noh, M. J. Rooks, G. S. Solomon, L. D. Negro, and H. Cao, Appl. Phys. Lett. **97**, 223101 (2010).

[12] C. Jin, X. Meng, B. Cheng, Z. Li, and D. Zhang, Phys. Rev. B **63**, 195107 (2001).

[13] J. Ballato, J. Dimaio, A. James, and E. Gulliver, Appl. Phys. Lett. **75**, 1497 (1999).

[14] C. Rockstuhl, U. Peschel, and F. Lederer, Opt. Lett. **31**, 1741 (2006).

[15] Y. Wang and S. Jian, Phys. Lett. A **352**, 550 (2006).

[16] C. Rockstuhl and F. Lederer, Phys. Rev. B **79**, 132202 (2009).

[17] M. Rechtsman, A. Szameit, F. Dreisow, M. Heinrich, R. Keil, S. Nolte, and M. Segev, arXiv:1012.3239.

[18] K. Edagawa, S. Kanoko, and M. Notomi, Phys. Rev. Lett. **100**, 013901 (2008).

[19] M. Florescu, S. Torquato, and P. J. Steinhardt, PNAS **106**, 20658 (2009).

[20] J.-K. Yang, C. Schreck, H. Noh, S.-F. Liew, M. I. Guy, C. S. O'Hern, and H. Cao, Phys. Rev. A **82**, 053838 (2010).

[21] S. Imagawa, K. Edagawa, K. Morita, T. Niino, Y. Kagawa, and M. Notomi, Phys. Rev. B **82**, 115116 (2010).

[22] P. D. García, R. Sapienza, Á. Blanco, and C. López, Adv. Mater. **19**, 2597 (2007).

[23] L. F. Rojas-Ochoa, J. M. Mendez-Alcaraz, J. J. Sáenz, P. Schurtenberger, and F. Scheffold, Phys. Rev. Lett. **93**, 073903 (2004).

[24] R. O. Prum, in *Bird coloration*, Vol. 1 (Harvard University Press, 2006) pp. 295–353.

[25] H. Noh, S. F. Liew, V. Saranathan, S. G. J. Mochrie, R. O. Prum, E. R. Dufresne, and H. Cao,

Adv. Mater. **22**, 2871 (2010).

[26] M. Harun-Ur-Rashid, A. Bin Imran, T. Seki, M. Ishii, H. Nakamura, and Y. Takeoka, ChemPhysChem **11**, 579 (2010).

[27] J. D. Forster, H. Noh, S. F. Liew, V. Saranathan, C. F. Schreck, L. Yang, J.-G. Park, R. O. Prum, S. G. J. Mochrie, C. S. O'Hern, H. Cao, and E. R. Dufresne, Adv. Mater. **22**, 2939 (2010).

[28] Y. Takeoka, M. Honda, T. Seki, M. Ishii, and H. Nakamura, ACS Appl. Mater. Interfaces **1**, 982 (2009).

[29] K. Ueno, A. Inaba, Y. Sano, M. Kondoh, and M. Watanabe, Chem. Commun., 3603(2009).

[30] I. Lee, D. Kim, J. Kal, H. Baek, D. Kwak, D. Go, E. Kim, C. Kang, J. Chung, Y. Jang, S. Ji, J. Joo, and Y. Kang, Adv. Mater. **22**, 4973 (2010).

[31] S. Fraden and G. Maret, Phys. Rev. Lett. **65**, 512 (1990).